Journal of Solid State Chemistry 183 (2010) 744–751

Contents lists available at ScienceDirect

Journal of Solid State Chemistry

journal homepage: www.elsevier.com/locate/jssc

Mn_3O_4 nanoplates and nanoparticles: Synthesis, characterization, electrochemical and catalytic properties

Khalid Abdelazez Mohamed Ahmed [a,b], Qiumei Zeng [a], Kangbing Wu [a], Kaixun Huang [a,*]

[a] Hubei Key Laboratory of Bioinorganic Chemistry & Materia Medica, School of Chemistry and Chemical Engineering, Huazhong University of Science and Technology, Wuhan 430074, PR China

[b] Department of Chemistry, School of Chemistry and Chemical Technology, Faculty of Science and Technology, Al-Neelain University, P.O. Box 12702, Khartoum, Sudan

ARTICLE INFO

Article history:
Received 3 October 2009
Received in revised form
14 January 2010
Accepted 16 January 2010
Available online 25 January 2010

Keywords:
Trimanganese tetraoxide
Nanoplates
Nanoparticles
Electrochemical
Catalysis

ABSTRACT

Mn_3O_4 hexagonal nanoplates and nanoparticles were synthesized via a solvent-assisted hydrothermal oxidation process at low temperature and a solvothermal oxidation method, respectively. The synthesized product was characterized by powder X-ray diffraction (XRD), field emission scanning electron microscopy (FESEM), transmission electron microscopy (TEM), high resolution transmission electron microscopy (HRTEM), electron diffraction (ED), Fourier transform infrared (FT-IR) spectroscopy. Their capability of catalytic oxidation of formaldehyde to formic acid at room temperature and atmospheric pressure and electrochemical properties by cyclic voltammogram (CV) were compared. The results showed that Mn_3O_4 hexagonal nanoplate is a better catalyst, and the hexagonal nanoplates and nanoparticles modified electrodes blended with carbon black have a higher specific capacitance.

1. Introduction

Nanomaterials feature high surface energy and reactivity resulting from their high specific surfaces and exhibit special electric, magnetic, absorptive, and catalytic properties [1–6]. Manganese oxide nanomaterials, with notably increased surface area and greatly reduced size, are of great importance due to their wide-range applications [7–9]. Brock et al summarized the electrochemical and catalytic applications of manganese oxides. One of the most important industrial applications of manganese oxides is oxidation catalysis [10]. In particular, the studies with manganese oxides on environmental reactions such as ozone decomposition, oxidation of organic pollutants, reduction of nitric oxide, and NO and NO_2 decomposition have been focused. Mn_3O_4 is known to be an effective catalyst to limit the emission of NO_x and CO, or oxidation ethanol [11,12]. In addition, Mn_3O_4 nanomaterials as a potential capacitor material were studied [13–15].

The properties of semiconductor nanostructured materials depend not only on their chemical composition but also on their shape and size. Mn_3O_4 was often synthesized by the high-temperature calcination of either higher manganese oxides (MnO_2, Mn_5O_8, and Mn_2O_3), or Mn^{II} and Mn^{III} oxysalts, hydroxides, or hydroxyoxides [16]. In the last decade, various different shape and size Mn_3O_4 nanocrystals have been synthesized by various techniques, for instance, single-crystal Mn_3O_4 nanorods were obtained by a simple chemical method [17]; polyhedral nanocrystals were prepared by a microwave-assisted solution-based method [18]; nanoparticles were prepared by oxidation precipitation method [19,20], vapor phase growth [21] and thermal decomposition [22,23]; hierarchical structure with radiated spherulitic nanorods was prepared via a simple solution-based coordinated route, or under mild and organic free template [24,25]; porous hexagonal plates were prepared by a hydrothermal method [26]; thin films were prepared by chemical bath deposition [27]; nanofibers were prepared by sol–gel process [28]; three-dimensional nanostructures were synthesized by soft chemistry templating process [29]. However, the exploration of low-temperature routes for the synthesis of Mn_3O_4 has, therefore, been worth attempting. Recently, nanocrystals like rods were obtained by one-step room-temperature synthesis [12] or by hydrothermal and solvothermal process [30,31], γ-Mn_3O_4 nanorods were also gained by one-step low-temperature alcohol–water thermal route [32], the uniform and ligand-capped nanocrystals with hausmannite structure could be prepared from MnO by controlled chemical oxidation [33,34].

Herein, we report the synthesis and characterization of two shapes of manganese oxide nanomaterials with polycrystalline structures: hexagonal nanoplates via a solvent-assisted hydrothermal oxidation process and nanoparticles via a solvothermal route, and compare their difference of electrochemical characterization and catalytic oxidation of formaldehyde to formic acid at room temperature and atmospheric pressure.

* Corresponding author. Fax: +86 27 8754 3632.
E-mail address: hxxzrf@mail.hust.edu.cn (K. Huang).

0022-4596/$ - see front matter © 2010 Elsevier Inc. All rights reserved.
doi:10.1016/j.jssc.2010.01.015

2. Experimental procedures

2.1. Materials

$MnCl_2 \cdot 4H_2O$ (99%), ammonium hydroxide (25–28%), potassium hydroxide, methyl orange, formaldehyde (37–40%), ethanol glycol (95%), manganese acetate tetrahydride, ethanol absolute (99%), n-butylamine (98.5%), graphite powder (spectral reagent) and paraffin oil were purchased from Sinopharm Group Chemical Reagent Co., Ltd., China.

2.2. Synthesis of hexagonal nanoplates

In a typical procedure, 3.13 mmol $MnCl_2 \cdot 4H_2O$ was dissolve in 50 ml distilled water. Then, 30 ml ammonium hydroxide solution (0.15 M) was added to the manganese chloride solution under continuous stirring, then 5 ml NaOH (1.2 M) was slowly added dropwise to the above solution. The pH value of this system was about 12. Then the sample was transferred to a flask and heated under reflux at 80 °C for 3 h. The brown precipitate was collected by centrifugation at 8000 rpm for 10 min and washed with distilled water and absolute ethanol several times to remove the excessive reactants and byproducts, followed by drying in a vacuum at 60 °C for 14 h and the brown precipitates were collected for characterization.

2.3. Synthesis of nanoparticles

In this procedure, 2 mmol manganese acetate tetrahydride and 1 mmol n-butylamine were dissolved in 10 mL deionization water, 50 mL absolute ethanol was added and stirred at room temperature for 15 min, 0.8 mL KOH (2 M) was added under continuous stirring and the resulting solution was sealed into an 80 mL Teflon-lined stainless steel autoclave and heated at 180 °C for 14 h in an electric oven. The autoclave was cooled to room temperature naturally when the reaction time was finished. Brown product was collected by centrifugation at 8000 rpm for 10 min and washed with distilled water and absolute ethanol several times to remove the excessive reactants and byproducts, followed by drying in a vacuum at 60 °C for 14 h. The brown powders were collected for characterization.

2.4. Characterization

The X-ray diffraction (XRD) pattern of the products was recorded by employing a PANalytical B.V. (Philips) χ'Pert PRO XRD with Cu KR radiation at 1.54060 Å and a scanning rate of $0.02\ s^{-1}$. The FT-IR spectra of the products were obtained with an EQUINOX55 Burker FT spectrometer in the range 400–4000 m^{-1} at room temperature, with the sample in KBr disk. The morphology and size of as-prepared microstructure of the products were observed by FEI Sirion 200 field emission scanning electron microscopy (FE-SEM). The SAED and transmission electron microscopy (TEM) images were observed on a Tecnai G220 transmission electron microscopy. High-resolution transmission electron microscopy (HRTEM) images were carried out on a JEM-2010FEF TEM at an acceleration voltage of 200 kV. The partial degradation of formaldehyde measurement by ultraviolet–visible (UV–vis) absorption spectrum was recorded on (SHIMADZU kv) spectrometer.

2.5. Cyclic voltammograms

All electrochemical measurements were performed on a CHI610B electrochemical workstation (Shanghai Chenhua Co. Ltd., China) in a three-electrode system. The working electrode was a nano-Mn_3O_4 modified carbon paste electrode (CPE). A Pt wire and a saturated calomel electrode (SCE) were used as the counter and reference electrodes, respectively.

The Mn_3O_4 nanoplate-modified CPE (Mn_3O_4-NL/CPE) was prepared as follows: 20 mg Mn_3O_4 nanoplates and 100 mg graphite powder were mixed uniformly by milling in a small carnelian mortar, and then 25 μL paraffin oil was added into and milled again to give a homogenous modified carbon paste. After that, the resulting carbon paste was pressed into the end cavity (3 mm in diameter, 1 mm in depth) of the electrode body, and the surface was polished with a smooth paper. The Mn_3O_4 nanoparticles-modified CPE (Mn_3O_4-NP/CPE) was constructed in the same procedure. It is necessary to note that the amount of paraffin oil must be carefully controlled because excessive paraffin oil will lower the conductivity, while insufficient paraffin oil is not beneficial to obtain uniform Mn_3O_4 modified carbon paste.

2.6. Catalytic oxidation of aldehyde

The catalytic oxidation of aldehyde (formaldehyde or benzaldehyde) was carried out in a 250 mL three-neck flask at 30 °C under magnetic stirring; 2.4 mmol aldehyde was dissolved in 100 ml deionization water, then transferred to the flask and air as oxygen source was pumped by air pump. The absorption values of the solution were recorded at λ_{max} 464 nm by using UV–vis spectrometer. When 0.1 mmol Mn_3O_4 powder was added to the flask, timing began. Four ml of the solution was taken at different times, the catalyst powder was removed by filter paper, then 2 μmol of methyl orange was added to the solution, and the absorption values were recorded.

3. Results and discussion

3.1. Mn_3O_4 nanoplates

Fig. 1(a_1) shows the XRD spectrum of as-synthesized Mn_3O_4 hexagonal nanoplates. All of the diffraction peaks can be indexed to tetragonal phase structured Mn_3O_4 with a lattice constant (a=5.76 Å and c=9.47 Å), which is in good agreement with the standard data from JCPDS card (no. 024-0734) (Fig. 1(a_3)). No impurity phases can be detected. Fig. 1b shows Fourier transform infrared (FT-IR) spectrum of the as-prepared Mn_3O_4 product, displaying a notable resemblance to those of Mn_3O_4 obtained in previous studies [16,35,36]. In the region from 650 to 500 cm^{-1} of the observed spectrum, two absorption peaks were observed at 626.94 and 524.88 cm^{-1}, associated with the coupling modes between the Mn–O stretching modes of tetrahedral and octahedral sites. In the region from 500 to 400 cm^{-1}, one peak at 417.66 cm^{-1} is attributed to the band-stretching mode of the octahedral sites. Moreover, other peaks might come from absorbed water, ethanol (wash solvents) and ammonia. Therefore, the FT-IR spectra further confirms the formation of the product.

The morphologies of products were investigated by FE-SEM. The low-magnification FE-SEM morphology of the as-prepared product is shown in Fig. 2a and the sample consists of nanoplates in high quantity and homogeneousness; the high-magnification image is shown in Fig. 2b. The obtained products exhibit a hexagonal shape, and some nanoparticles are randomly adsorbed on the surface of nanoplates. The edge length of the nanoplate is around 100 nm and the thickness is about 10 nm. TEM image of Mn_3O_4 nanoplates is shown in Fig. 2c. The corresponding selected area ED pattern (inserted in Fig. 2c) revealed that the nanoplate was polycrystalline structure. More details of the nanoplates were

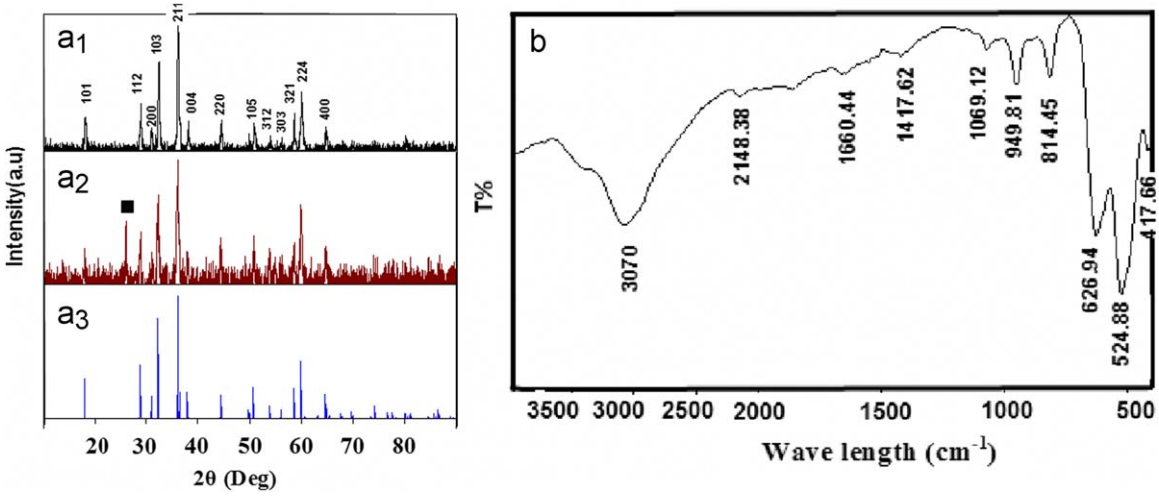

Fig. 1. XRD patterns of the materials. (a_1) Before catalytic reaction, (a_2) after catalytic reaction, and (a_3) the standard data from JCPDS card no. 024-0734, (b) FT-IR spectrum of the synthesized Mn_3O_4 hexagonal nanoplates; ■Mn_3O_4-JCPDS card no. 75-1560.

investigated by HRTEM. Fig. 2d is the HRTEM image of the Mn_3O_4 crystal nanoplates taken from Fig. 2c. The interplanar distance calculated from the lattice fringes of sample is 0.324 nm, almost in accordance with the {112} lattice distances of tetragonal Mn_3O_4. The ammonium hydroxide and NaOH were proved to play an important role for the formation of trimanganese tetraoxide hexagonal nanoplates. When ammonium hydroxide or sodium hydroxide was canceled under the same conditions, as shown in Fig. 2e and f, the smaller nanoparticles were obtained.

In this preparation, the chemical reactions to obtain as-synthesized hexagonal nanoplates may be formulated as follows:

$$MnCl_2 + 2NH_4OH \rightarrow Mn(OH)_2 + 2NH_4Cl$$

$$Mn^{2+} + nNH_3 \leftrightarrow Mn(NH_3)_n^{2+} \quad (n = 1-4)$$

$$6Mn^{2+} + O_2 + 12OH^- \rightarrow 2Mn_3O_4 + 6H_2O$$

Coordination compound of manganese ammoniate might play a role in controlling not only release velocity of Mn^{2+} ions, but also growth direction of Mn_3O_4 nanocrystal. Recently the effects of pH and ammonia on the Mn_3O_4 morphology were investigated [22,37]. We believe that excessive NH_3 as the ligands were adsorbed on two surfaces of nanaoparticle and played a role of capping agent, suppressing the growth rate of two planes. As a result, the edge of nanoplate covered with the fewest NH_3 molecules grew fastest and nanaoplates were formed.

3.2. Mn_3O_4 nanoparticles

To compare the effects of different shapes and sizes on the electrochemical properties and catalytic oxidation of formaldehyde to formic acid, another nanomaterial, Mn_3O_4 nanoparticle, was prepared. A typical XRD pattern of the as-synthesized Mn_3O_4 nanoparticles from manganese acetate tetrahydride, n-butylamine and potassium hydroxide through solvothermal process at 180 °C for 14 h is shown in Fig. 3(a_1). All diffraction peaks can be indexed to tetragonal phase structure of Mn_3O_4 with a lattice constant (a=5.765 and 9.442 Å), which is in agreement with the standard data from JCPDS card no. 80-0382 in Fig. 3(a_3). The FT-IR spectrum of nanoparticles is showed in Fig. 3b. Similar to nanoplates, there were three peaks at 412.26, 530.93 and 636.61 cm^{-1} in the spectra region from 650 to 400 cm^{-1}, confirming that the product was Mn_3O_4. Analogously, there were interactions between organic molecules and nanoparticles. The bands at 1550–1514, 1453 and 1358 cm^{-1} could be ascribed to the C–H bending vibrations and absorption at 1122.77 cm^{-1} matches the C–N stretching. The broad bands centered at 3400 and 2927 cm^{-1} are assigned to the O–H stretching and bending modes of water.

The morphologies of the as-prepared products were examined by FE-SEM. The panoramic morphology of the sample (Fig. 4a) shows that the sample consists of nanoparticles in high quantity and homogeneousness. The high-magnification image and TEM image of the sample shown in Fig. 4b and c indicate that the average size of the nanoparticles is around 30 nm. Corresponding selected area ED pattern (inserted in Fig. 4c) indicates that the Mn_3O_4 nanoparticles were also polycrystalline structure. The high-resolution TEM (HRTEM) image of the Mn_3O_4 nanoparticle is shown in Fig. 4d, the calculated interplanar distance is about 0.483 and 0.273 nm, which correspond to {101} and {103} planes of particle Mn_3O_4, respectively. Partial Mn^{+2} were oxidated into Mn^{+3} due to limited existence of oxygen in the autoclave under such basic condition and Mn_3O_4 nanoparticles were formed.

In this synthesis system, the n-butylamine ligands have great effects on the morphology of the final nanoparticles. When n-butylamine was canceled under the same conditions, as shown in Fig. 4e, the morphology of the final nanoparticles was changed and the smaller nanoparticles were obtained.

3.3. Electrochemical properties

The electrochemical properties of Mn_3O_4 nanoplates (NL) and nanoparticles (NP) modified CPE electrodes (Mn_3O_4-NL/CPE and Mn_3O_4-NP/CPE) were characterized using the probe of $K_3[Fe(CN)_6]$. Figs. 5a and b depict the cyclic voltammograms of $K_3[Fe(CN)_6]$ at CPE and the Mn_3O_4-NL/CPE or Mn_3O_4-NP/CPE. From the comparison, it is apparent that the electrochemical responses of $K_3[Fe(CN)_6]$ are greatly improved at Mn_3O_4-NL/CPE and Mn_3O_4-NP/CPE. On one hand, the reduction peak potential shifts positively, and the oxidation peak potential shifts negatively, suggesting that Mn_3O_4-NL or Mn_3O_4-NP exhibits catalytic activity to the reduction of $K_3[Fe(CN)_6]$. On the other hand, the reduction and oxidation peak currents remarkably increase, which is consistent with marked increase of surface area of modified CPE. According to Randles–Sevcik equation ($i_p=(2.687\times10^5)n^{3/2}v^{1/2}D^{1/2}AC$), the effective surface area of unmodified CPE is about 0.041 cm^2, however, the effective surface area of Mn_3O_4-NL/CPE and Mn_3O_4-NP/CPE is 0.196 and

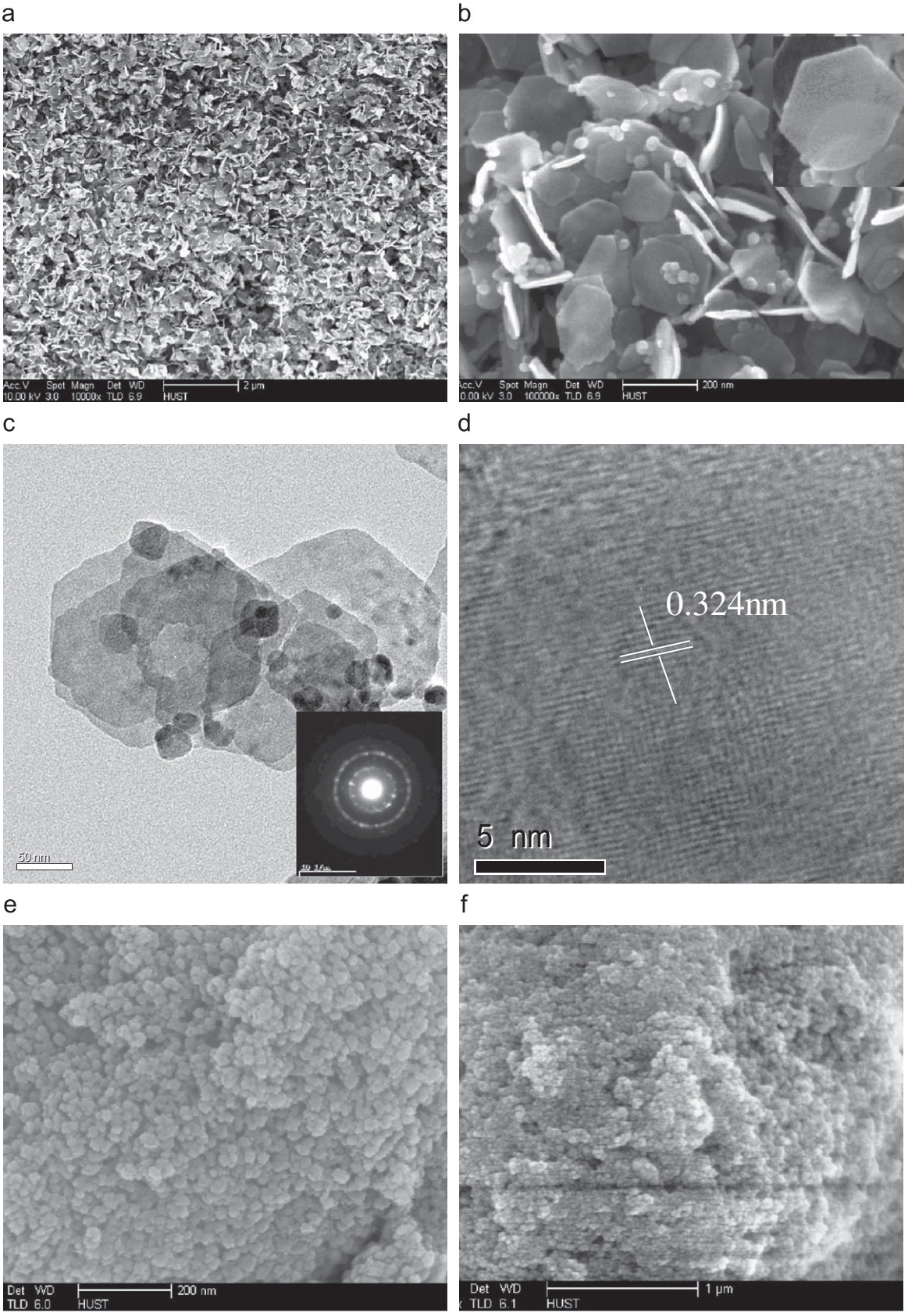

Fig. 2. (a) Representative SEM images, (b) high-magnification SEM images, (c) TEM images (insert, a selected area electron diffraction pattern), (d) HR-TEM images of the Mn_3O_4 nanoplates prepared by oxidation-reflux method at 80 °C for 3 h, (e) and (f) FE-SEM images of the as-prepared product without ammonia and sodium hydroxides under the same conditions.

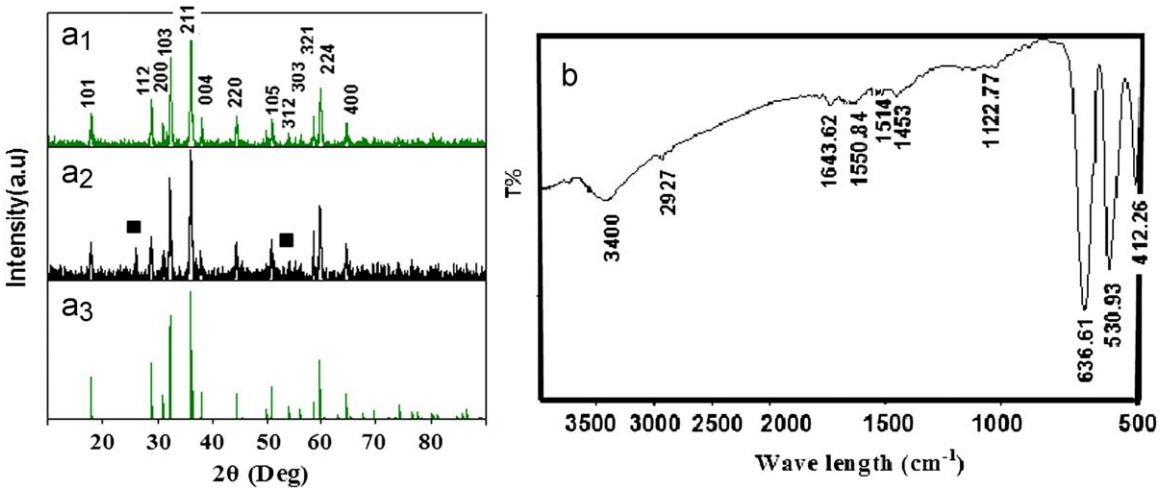

Fig. 3. XRD patterns of the materials. (a_1) Before catalytic reaction, (a_2) after catalytic reaction, and (a_3) the standard data from JCPDS card no. 80-0382, (b) FT-IR spectrum of the synthesized Mn3O4 nanoparticles; ■Mn_3O_4-JCPDS card no. 75-0765.

0.194 cm^2, respectively, which is more than 4.7 times of that of CPE. This result indicates that Mn_3O_4-NL and Mn_3O_4-NP possess notable surface enhancement effect.

However, both modified electrodes exhibit similar current responses in their CVs (Fig. 5c). The specific capacitance of the electrodes can be obtained by the following equation [38]:

$$C(\mathrm{F/g}) = \frac{Q}{\Delta E \cdot m}$$

where Q is the voltammetric charge, ΔE is the voltage window, and m is the mass of the material of the electrode. The specific capacitance of Mn_3O_4 hexagonal nanoplates modified CPE is about 237 Fg^{-1} and the specific capacitance of Mn_3O_4 nanoparticles electrode is about 226 Fg^{-1}.

3.4. Partial oxidation of the formaldehyde

The oxidation of formaldehyde by Mn_3O_4 nanocrystals in aqueous solutions is illustrated by UV–vis spectrometer (Fig. 6(a_1)). Three curves (curve I, II, III) represent without catalyst, with Mn_3O_4 nanoparticles, and with Mn_3O_4 nanoplates, respectively. We can see the value of absorption without change in curve I and a little increase in curve II with the increase of reaction time. However, in curve III, the value of absorption increases observably with the increase of reaction time and, in these cases, formaldehyde as reducing agent was oxidated into formic acid by oxygen under catalysis of Mn_3O_4 nanoplates.

$$CH_2O + 1/2O_2 \xrightarrow{Mn_3O_4} HCOOH$$

The mechanism of this reaction can be considered a pseudo first order (excess oxygen). According to the rate constant formula ($k=(2.303/t)\log(A_o/A_t)$), the rate constant of formaldehyde oxidation catalyzed by Mn_3O_4 nanoplates is about $2.9\times10^{-2}\,\mathrm{min}^{-1}$ (Fig. 6(b_1)), and by Mn_3O_4 nanoparticles is $0.96\times10^{-2}\,\mathrm{min}^{-1}$ (Fig. 6 (c_1)).

To compare the catalytic activities of Mn_3O_4 nanocrystal for the oxidations of other substrates besides CH_2O, the oxidation of benzaldehyde under the same procedures and conditions was studied. As shown in Fig. 6(a_2), the three curves (curve A, B and C) represent without catalyst, with Mn_3O_4 nanoparticles, and with Mn_3O_4 nanoplates, respectively. Compared with the oxidation of formaldehyde, the difference of the catalytic activity of nanoparticles and nanoplates for the oxidations of benzaldehyde is smaller. It could be related with solubility of benzaldehyde. The rate constant of the catalytic oxidation of benzaldehyde by Mn_3O_4 nanoplates is about $5.67\times10^{-3}\,\mathrm{min}^{-1}$ (Fig. 6(b_2)) and is about $4.895\times10^{-3}\,\mathrm{min}^{-1}$ by Mn_3O_4 nanoparticles (Fig. 6(c_2)).

The morphology of the Mn_3O_4 nanoplates and nanoparticles after catalytic oxidation of formaldehyde were examined by FE-SEM, as shown in Fig. 7. Before and after the catalytic oxidation of formaldehyde, there are changes significantly in morphologies for Mn_3O_4 hexagonal nanoplates and nanoparticles. The hexagonal nanoplates and nanoparticles all were broken into pieces. Furthermore, their crystallite structures after the catalytic oxidation of formaldehyde were studied by XRD patterns, all the diffraction peaks can be indexed to tetragonal phase of Mn_3O_4 according to JCPDS 24-0734 for nanoplates and JCPDS card no. 80-0382 for nanoparticles except lesser peaks (Fig. 1(a_2) and Fig. 3(a_2)).

In general, the catalytic activity of materials is connected with their surface areas. However, Mn_3O_4 nanoparticles and nanoplates have almost same effective surface area on the modified CPE electrodes from above calculation. Therefore, similar to Zhang et al. results [39], it may be speculated that the Miller-index of the crystal plays an important role in the catalytic activity of nanoparticles and nanoplates for the oxidations of aldehyde.

4. Conclusions

In this work, trimanganese tetraoxide (hausmannite) nanocrystals with different shapes, hexagonal nanoplates and nanoparticles, were successfully synthesized by a solvent-assisted hydrothermal oxidation process at low temperature and a solvothermal oxidation method, respectively. Mn_3O_4 hexagonal nanoplates have an average diameter around 170 nm, with the thickness of about 10 nm, while average size of the nanoparticles is about 30 nm. Mn_3O_4 nanoplates have a higher activity of catalytic oxidation of formaldehyde to formic acid than nanoparticles in aqueous solution at room temperature, speculating that the Miller-index of the crystal plays an important role in the catalytic activity of nanoplates and nanoparticles for the oxidations of aldehyde. The cyclic voltammograms show the hexagonal nanoplates and nanoparticles modified electrodes blended with carbon black have a higher specific capacitance.

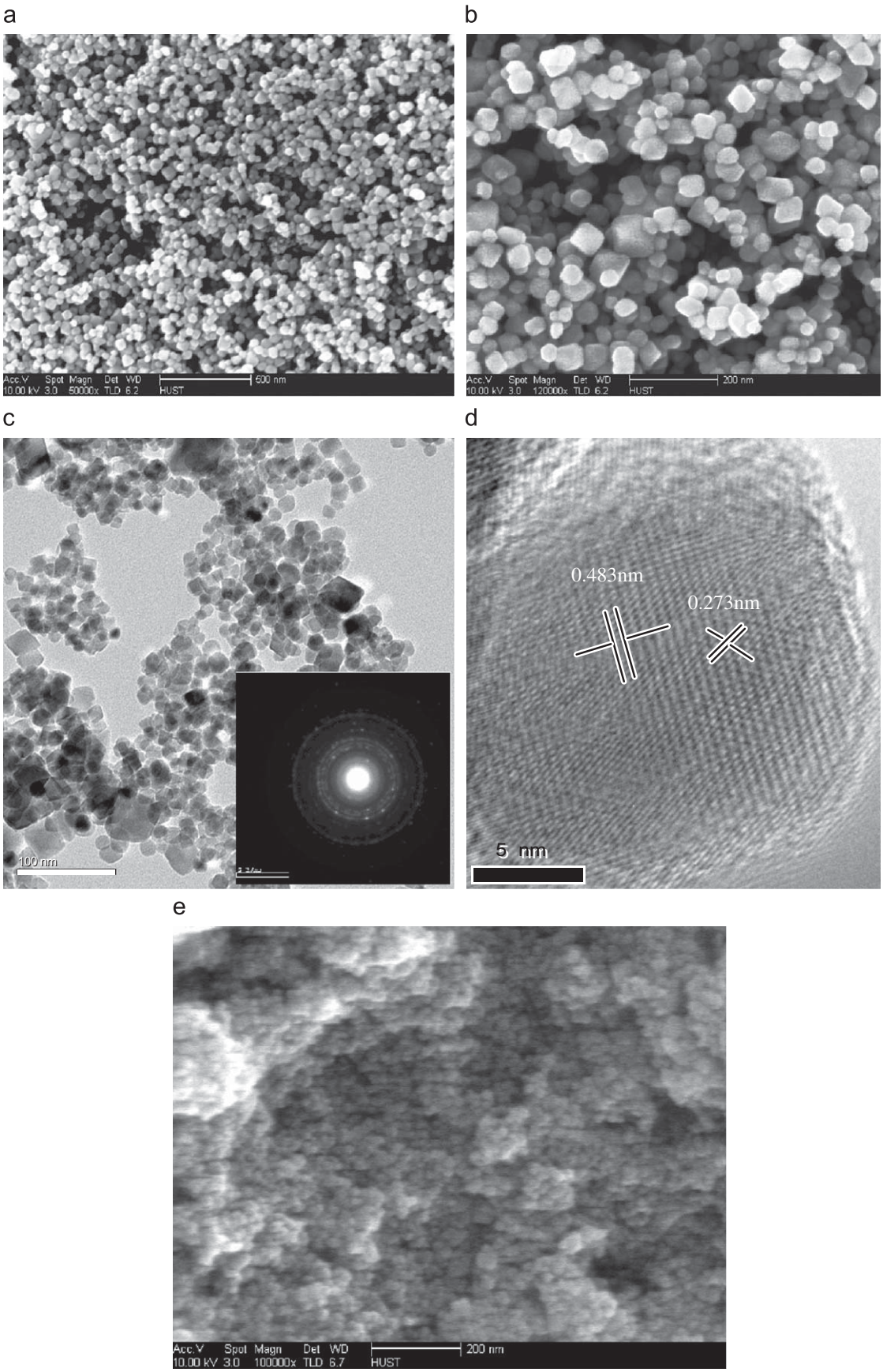

Fig. 4. (a) FE-SEM panoramic images, (b) FE-SEM magnification images, (c) TEM images (inserted, a selected area ED pattern), (d) HR-TEM images of Mn_3O_4 nanoparticles as-prepared through solvothermal process at 180 °C for 14 h, (e) FE-SEM images of as-prepared product without n-butylamine under the same conditions.

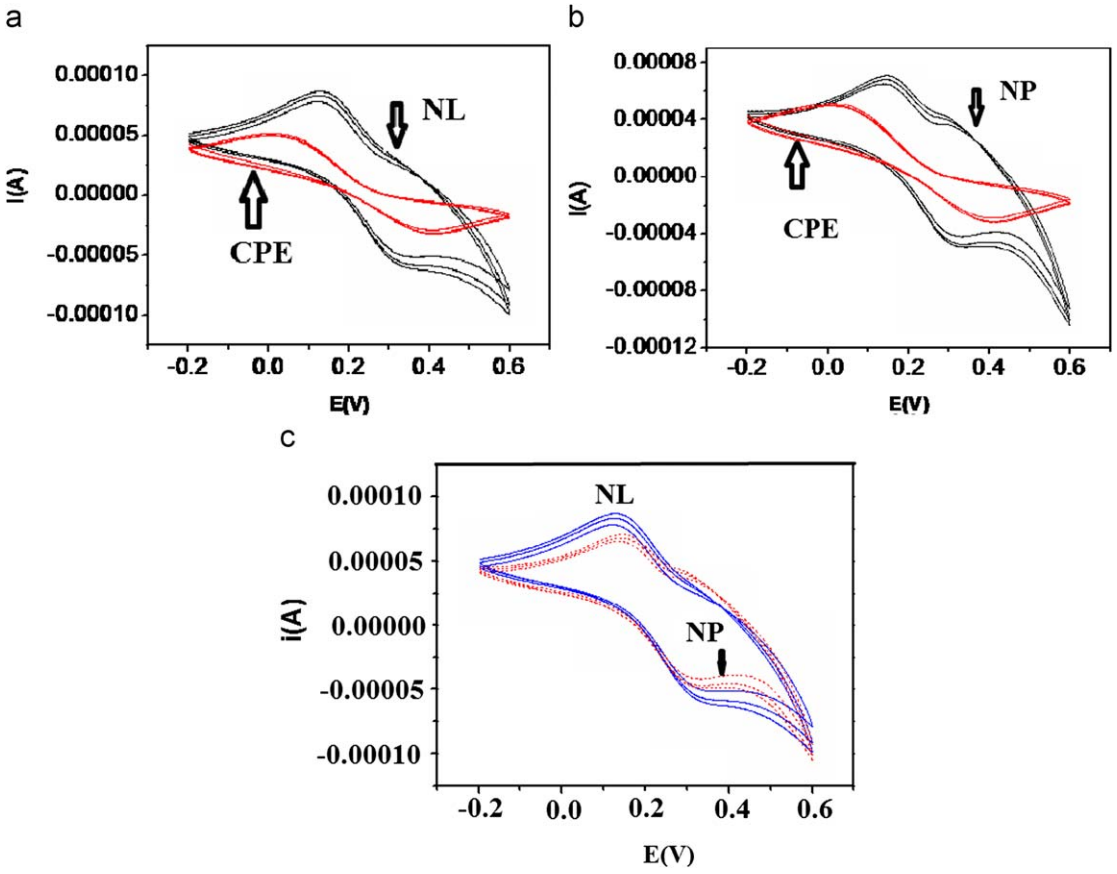

Fig. 5. Cyclic voltammograms of Mn_3O_4 nanocrystals modified CPE electrodes. (a) Comparison of nanoplate electrode (NL) with CPE electrode, (b) comparison of nanoparticle electrode (NP) with CPE electrode, (c) comparison of NP with NP.

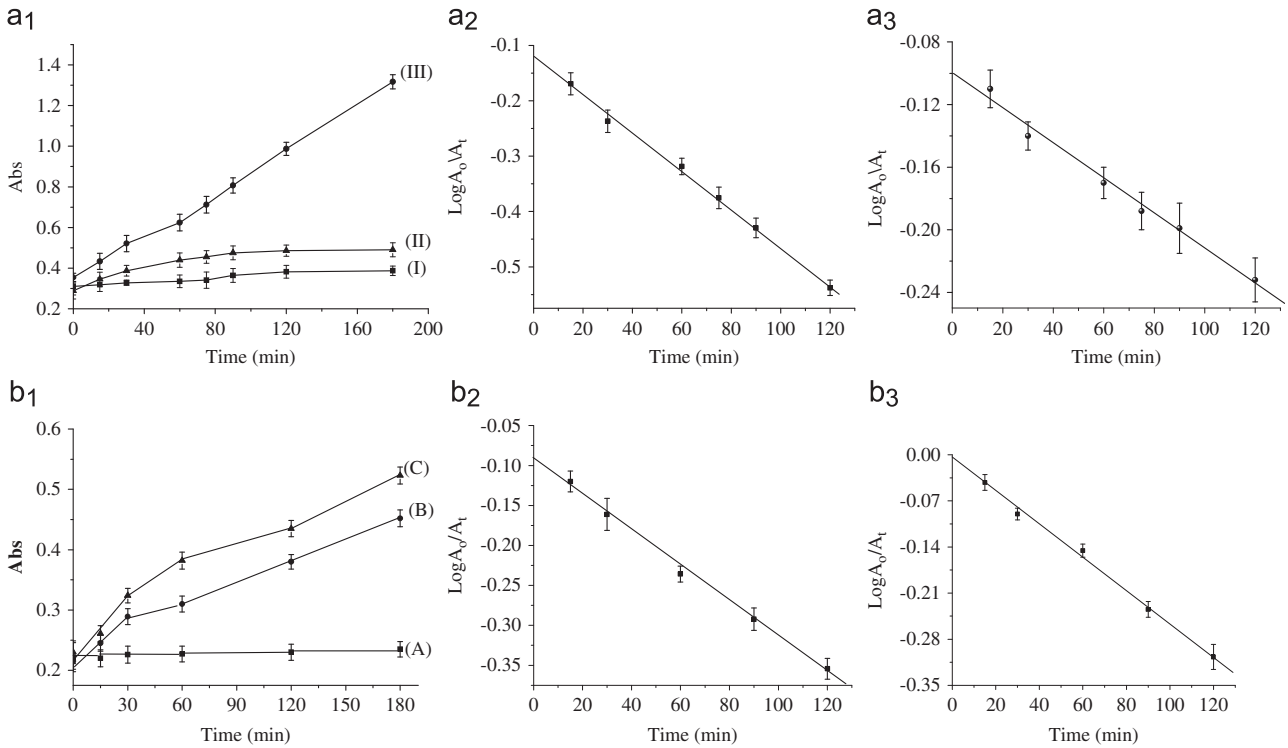

Fig. 6. The oxidation of aldehyde by Mn_3O_4 nanocrystals in aqueous solutions. (a_1) CH_2O+O_2 (I), $CH_2O+O_2+Mn_3O_4$ nanoparticles (II), $CH_2O+O_2+Mn_3O_4$ nanoplates (III); (a_2) and (a_3) the oxidation rate of formaldehyde oxidation to formic acid by Mn_3O_4 nanoplates and nanoparticles; (b_1) benzaldehyde+O_2 (A), benzaldehyde+Mn_3O_4 nanoparticles (B), benzaldehyde+Mn_3O_4 nanoplates (C); (b_2) and (b_3) the oxidation rate of benzaldehyde oxidation to benzoic acid by Mn_3O_4 nanoplates and Mn_3O_4 nanoparticles; all data were repeated 3 times.

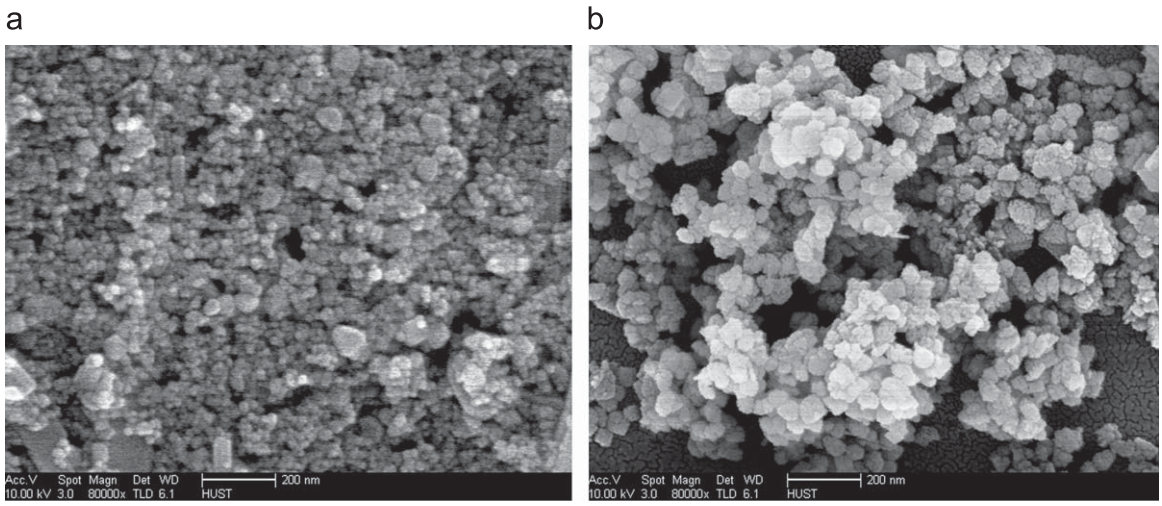

Fig. 7. FE-SEM images of the Mn_3O_4 nanocrystals after catalytic oxidation of formaldehyde. (a) Mn_3O_4 nanoplates, (b) Mn_3O_4 nanoparticles.

Acknowledgments

We thank the faculty from the Analysis and Test Center of Huazhong University of Science and Technology for the technical assistance on characterization. This research was supported by MOST 973 program (Project no. 2006CB705606a).

References

[1] J.Q. Pan, Y.Z. Sun, Z.H. Wang, P.Y. Wan, X.G. Liu, M.H. Fan, J. Mater. Chem. 17 (2007) 4820–4825.
[2] H. Huang, S.C. Yin, T. Kerr, N. Taylor, L.F. Nazar, Adv. Mater. 14 (2002) 1525–1528.
[3] X. Wang, Y. Li, J. Am. Chem. Soc. 124 (2002) 2880–2881.
[4] G. Jain, J. Yang, M. Balasubramanian, J.J. Xu, Chem. Mater. 17 (2005) 3850–3860.
[5] W.P. Tang, X.J. Yang, Z.H. Liu, K. Ooi, J. Mater. Chem. 13 (2003) 2989–2995.
[6] D. Zitoun, N. Pinna, N. Frolet, C. Belin, J. Am. Chem. Soc. 127 (2005) 15034–15035.
[7] W. Zhang, Z. Yang, Y. Liu, S. Tang, X. Han, M.J. Chen, J. Cryst. Growth 263 (2004) 394–399.
[8] G. Zhou, F. Rong, C. Xian-Hui, W. Yi-Cheng, Inorg. Chem. Commun. 4 (2001) 294–296.
[9] Z. Weixin, W. Cheng, Z. Xiaoming, X. Yi, Q. Yitai, Solid State Ionics 117 (1999) 331–334.
[10] S.L. Brock, N. Duan, Z.R. Tian, O. Giraldo, H. Zhou, S.L. Suib, Chem. Mater. 10 (1998) 2619–2628.
[11] Y.-F. Han, F.-X. Chen, K. Ramesh, Z.-Y. Zhong, E. Widjaja, L.-W. Chen, Appl. Catal. B: Environ. 76 (2007) 227–234.
[12] A.V. Olmos, R. Redon, G.R. Gattorno, M.E.M. Zamora, F.M. Leal, A.L.F. Osorio, J.M. Saniger, J. Colloid Sci. 291 (2005) 175–180.
[13] S.C. Pang, M.A. Anderson, T.W. Chapman, J. Electrochem. Soc. 147 (2000) 444–450.
[14] K.W. Nam, K.B. Kim, J. Electrochem. Soc. 153 (2006) 81–88.
[15] J.K. Chang, W.T. Tsai, J. Electrochem. Soc. 150 (2003) 1333–1338.
[16] F.A. Al Sagheer, M.A. Hasan, L. Pasupulety, M.I. Zaki, J. Mater. Sci. Lett. 18 (1999) 209–211.
[17] Z.H. Wang, D.Y. Geng, Y.J. Zhang, Z.D. Zhang, J. Cryst. Growth 310 (2008) 4148–4151.
[18] L.-X. Yang, Y.-J. Zhu, H. Tong, W.-W. Wang, G.-F. Cheng, J. Solid State Chem. 179 (2006) 1225–1229.
[19] T. Ozkaya, A. Baykal, H. Kavasb, Y. Koseoglu, M.S. Toprak, J. Physica B 403 (2008) 3760–3764.
[20] Z.W. Chen, J.K.L. Lai, C.H. Shek, Scripta Materialia 55 (2006) 735–738.
[21] Y.Q. Chang, X.Y. Xu, X.H. Luo, C.P. Chen, D.P. Yu, J. Cryst. Growth 264 (2004) 232–236.
[22] M. Salavati-Niasari, F. Davar, M. Mazaheri, Polyhedron 27 (2008) 3467–3471.
[23] W.S. Seo, H.H. Jo, K. Lee, B. Kim, S.J. Oh, J.T. Park, Angew. Chem. Int. Ed. Eng. 43 (2004) 1115–1117.
[24] Z. Wu, K. Yu, Y. Huang, C. Pan, Y. Xie, J. Chem. Cent. 1 (2007) 1–9.
[25] J. Yuan, W.N. Li, S. Gomez, S.L. Suib, J. Am. Chem. Soc. 127 (2005) 14184–14185.
[26] T.Z. Ren, Z.Y. Yuan, W. Hu, X. Zou, Micropor. Mesopor. Mater. 112 (2008) 467–473.
[27] H.Y. Xu, S.L. Xu, X.D. Li, H. Wang, H. Yan, J. Appl. Surf. Sci. 252 (2006) 4091–4096.
[28] C. Shao, H. Guan, Y. Liu, X. Li, X. Yang, J. Solid State Chem. 177 (2004) 2628–2631.
[29] C. Du, J. Yun, R.K. Dumas, X. Yuan, K. Liu, N.D. Browning, N. Pan, Acta Materialia 56 (2008) 3516–3522.
[30] Z. Yang, Y. Zhang, W. Zhang, X. Wang, Y. Qian, X. Wen, S. Yang, J. Solid State Chem. 179 (2006) 679–684.
[31] Y.C. Zhang, T. Qiao, X.Y. Hu, J. Solid State Chem. 177 (2004) 4093–4097.
[32] B. Yang, H. Hu, C. Li, X. Yang, Q. Li, Y. Qian, Chem. Lett. 33 (2004) 804–805.
[33] M. Yin, S. O'Brien, J. Am. Chem. Soc. 125 (2003) 10180–10181.
[34] I. Rusakova, T. Ould-Ely, C. Hofmann, D. Prieto-Centurion, C.S. Levin, N.J. Halas, A. Luettge, K.H. Whitmire, Chem. Mater. 19 (2007) 1369–1375.
[35] W. Wang, C. Xu, G. Wang, Y. Liu, C. Zheng, Adv. Mater. 14 (2002) 837–840.
[36] M. Ishii, M. Nakahira, J. Solid State Commun. 11 (1972) 109–212.
[37] D.P. Dubal, D.S. Dhawale, R.R. Salunkhe, S.M. Pawar, V.J. Fulari, C.D. Lokhande, J. Alloys Compd. 484 (2009) 218–221.
[38] H. Xia, W. Xiao, M.O. Lai, L. Lu, Nanoscale Res. Lett. 4 (2009) 1035–1040.
[39] L. Zhang, Q. Zhou, Z. Liu, X. Hou, Y. Li, Y. Lv, Chem. Mater. 21 (2009) 5066–5071.